AIAA SciTech Forum
January 3-7, 2022, San Diego, CA & Virtual
AIAA SCITECH 2022 Forum

10.2514/6.2022-2536

Aerodynamic Analysis of a Slotted, Natural-Laminar-Flow Transonic Trussed-Braced Wing Aircraft Configuration

Cody Perkins[*] Zhi Yang[†] Ilker Topcuoglu[‡] and Dimitri Mavriplis[§]
University of Wyoming, Laramie, WY 82070, United States

James G. Coder[¶] and Ethan Hereth[‖]
University of Tennessee, Knoxville, TN 37996, United States

Chris Axten[**]
Penn State University, University Park, PA 16802, United States

The integration of a slotted, natural-laminar-flow (SNLF) airfoil with a transonic, truss-braced wing (TTBW) configuration has been shown to offer significant benefits in comparison to other widely implemented designs for commercial transport applications. This work focuses on the computational aerodynamic analysis of an S207 SNLF TTBW vehicle flying at cruise conditions, with the study being supplemented by independent results of the S207 profile in two dimensions. The performance of the wing is largely dependent on the duration of laminar flow maintained across the chord length. Thus proper prediction of the transition from laminar to turbulent flow and its sensitivity to geometric changes is of top priority. Computations are performed in both two and three dimensions using Reynolds-averaged Navier-Stokes (RANS) solvers on unstructured grids with transition prediction models. Results in two dimensions agree well with the design performance metrics of the S207 SNLF airfoil, and also illustrate the sensitivity of this airfoil to flap positioning. Results in three dimensions were used to identify geometric inconsistencies in wing sweep transformations, which led to a redesign with improved performance. However, predicted transition locations on the current configuration occur earlier than expected by design, thus leading to less than optimal performance. CFD simulations point to the need for wing geometry modifications and/or alleviation of flow separation at the fuselage-wing fairing location.

I Introduction

Concern for the impact of global climate change continues to grow and with it comes the necessity to develop and implement long lasting improvements to aircraft technology. The NASA Aeronautics Mission Directorate has formulated six thrusts in response to drivers shaping the needs of the aviation industry,[1] each with their own near-term (N+1), mid-term (N+2), and far-term (N+3) metrics. The third thrust emphasizes goals for reduction in noise, emissions, and fuel consumption for transonic commercial aircraft with a vision for 2050 net emissions being 50% that of a 2005 baseline.

Slotted, natural-laminar-flow (SNLF) airfoils are an enabling technology for meeting N+3 performance criteria. Consisting of two elements, an SNLF wing takes advantage of a favorable gradient enabled by a relatively low pressure

[*]MS Student, Department of Mechanical Engineering, AIAA Member; Email: cperki12@uwyo.edu
[†]Research Scientist, Department of Mechanical Engineering, AIAA Member; Email: ZYang@uwyo.edu
[‡]Post-Doctorate Researcher, Department of Mechanical Engineering AIAA Member; Email: itopcuog@uwyo.edu
[§]Professor, Department of Mechanical Engineering, AIAA Associate Fellow; Email: mavripl@uwyo.edu
[¶]Assistant Professor, Department of Mechanical, Aerospace and Biomedical Engineering, AIAA Senior Member; Email: jcoder@utk.edu
[‖]Assistant Research Professor, Department of Mechanical, Aerospace and Biomedical Engineering, AIAA Member; Email: ehereth@utk.edu
[**]MS Student, Department of Aerospace Engineering, AIAA Member; Email: cja5217@psu.edu

at the slot exit to maintain extensive runs of laminar flow, theoretically achieving significantly lower profile drag in comparison to a natural-laminar-flow (NLF), single element airfoil. Furthermore, the concept is much less complex mechanically, structurally, and operationally than other profile drag reduction techniques such as active laminar flow control.[2] Studies conducted on already existing SNLF geometries offer testament to the technology's benefits. For example, the S414, proposed for rotorcraft applications, demonstrated through both computational analysis and wind tunnel testing better performance over its single element counterpart.[3,4]

The S207 is a 13.49%-thick SNLF airfoil designed for transonic commercial aircraft and has been shown computationally to meet high maximum lift and low profile drag goals.[2,5] The geometric profile of the S207 is shown in Figure 1. When paired with the drag reducing benefits of the transonic truss-braced wing (TTBW) configuration developed by Boeing,[6] another N+3 concept, predicted performance is significantly improved compared to modern aircraft.[7] Current efforts conducted under the Advanced Aerodynamic Design Center for Ultra-Efficient Commercial Vehicles, which is a NASA funded University Leadership Initiative (ULI) led by the University of Tennessee at Knoxville, are focused on the extensive analysis of this SNLF TTBW configuration, with a 70% reduction in fuel and energy burn compared to 2005 standards being the goal.[8]

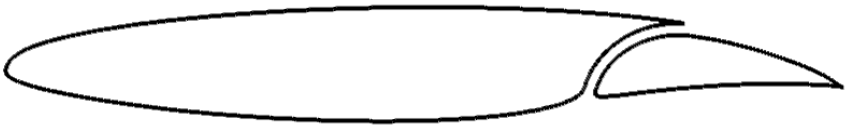

Figure 1: S207 SNLF Airfoil

The present work seeks to support the ULI through computational aerodynamic analysis of a collaboratively-designed S207-based vehicle. The performance of the vehicle at cruise conditions can be measured by success in maintaining large regions of laminar flow across the span of the wing. Flow physics that enable the transition from laminar to turbulent flow, such as adverse pressure gradients and shock waves, are greatly detrimental to fuel efficiency, making their prevention paramount. At the same time, transition behavior for SNLF configurations can be significantly affected by small geometrical changes. Thus, the ability to rapidly analyze multiple candidate configurations, possibly including the effect of structural deflections, takes on additional importance early in the design process. On the other hand, numerical transition prediction for applied aerodynamics is still under development. Potentially important flow physical effects such as cross-flow induced instabilities are often neglected, and robust convergence of free transition models within Reynolds-averaged Navier-Stokes CFD solvers can be problematic, particularly for cases with regions of separated flow.

In the following sections, we begin with a short description of the methodology and tools employed to computationally study the performance of the S207 airfoil and the corresponding SNLF TTBW configuration. A section is included which describes validation of the computational methods including free transition modeling, for both two and three-dimensional problems. In the Results section, CFD analysis of the S207 SNLF airfoil is first discussed, along with a flap position sensitivity study. This is followed by a description of the designed three-dimensional SNLF TTBW geometry and the predicted aerodynamic performance of two design iterations of this configuration. The paper concludes with remarks on progress made, but also persisting challenges and work to be completed.

II Methodology

The flow solvers employed for the work presented are NSU2D[9] and NSU3D.[10] Both codes are steady-state Reynolds-averaged Navier-Stokes methods which operate on unstructured meshes and are nominally second-order accurate in space. NSU2D and NSU3D employ a central difference discretization with added matrix-based dissipation and use an efficient multigrid scheme for accelerating convergence to steady state. A variety of turbulence models are available, although the single-equation Spalart-Allmaras (SA) model[11] has been used exclusively in all calculations performed for this paper. In particular, NSU3D has been extensively validated through its use in previous drag prediction, high-lift prediction and aeroelastic prediction workshops.[12–14] In recent years, free transition models have been implemented into

NSU2D and NSU3D. NSU2D is equipped with the two-equation amplification factor transport (AFT2) model developed by Coder,[15,16] and implemented by Yang et al.[17] NSU3D includes both the AFT2 model and the single-equation Mentor transition model.[18,19] In this work, results are obtained assuming fully turbulent flow (using the SA model exclusively) as well for predicted free transition cases (using one of the aforementioned transition models coupled to the SA turbulence model).

III Validation Efforts

Validation of the implemented transition models, as well as application of the optimization framework to SNLF technology has been conducted under the ULI. NSU2D was initially validated using the S204 SNLF airfoil.[17] The S204, a predecessor to the S207, was designed for business-jet applications and was refined and studied using the Eppler and MSES codes as specified in the original report.[20]

The low-drag bucket is an attribute unique to NLF airfoils, and by extension SNLF airfoils. It is characterized by the lowest drag values on the drag polar at which significant laminar flow is achieved. Beyond the upper and lower CL conditions delimiting the drag bucket, there exist regions of rapid drag increase. This is due to movement of the boundary-layer transition location further upstream, resulting in significant turbulence.[2] The low-drag bucket for the S204 is constrained by lift coefficient values of approximately *0.2* at the lower limit and *0.4* at the upper limit, with slight variations for different Reynolds numbers.[20] Figure 2 illustrates the NSU2D results computed with and without free transition compared to the design polar for $Mach = 0.5$ and $Re = 12e6$. A freestream turbulence intensity of *0.07%* was used for these calculations. A contour plot of eddy viscosity is included, and suggests laminar flow is maintained for a large percentage of the chord length. Close agreement is observed between published and NSU2D results, and adequate capture of the low-drag bucket is achieved.

The TU Braunschweig sickle wing transition experiment performed by Petzold and Radespiel[21] was selected as a validation case for the NSU3D-SA-Menter and AFT2 model performances in reference.[22] Results associated with both implementations were compared with those in reference[21,23] and are reproduced herein. Figure 15 illustrates the spanwise transition location computed by the NSU3D models compared to the behavior presented by Coder.[23] Likewise, Figure 16 depicts the lower surface contours. Overall, the transition locations predicted by both models with NSU3D are found to agree qualitatively with those presented by Coder,[23] although the lower surface transition locations appear slightly further downstream in the NSU3D results. In reference,[22] NSU3D was applied to a notional S204-based three-dimensional TTBW configuration with free transition, including the effects of coupled aero-structural displacements. The code was subsequently used in a wing twist distribution optimization exercise with free transition[22] including the effects of structural displacements.[24] Although NSU3D has the capabilities for aero-structural analysis and optimization, these were not exercised in the current work.

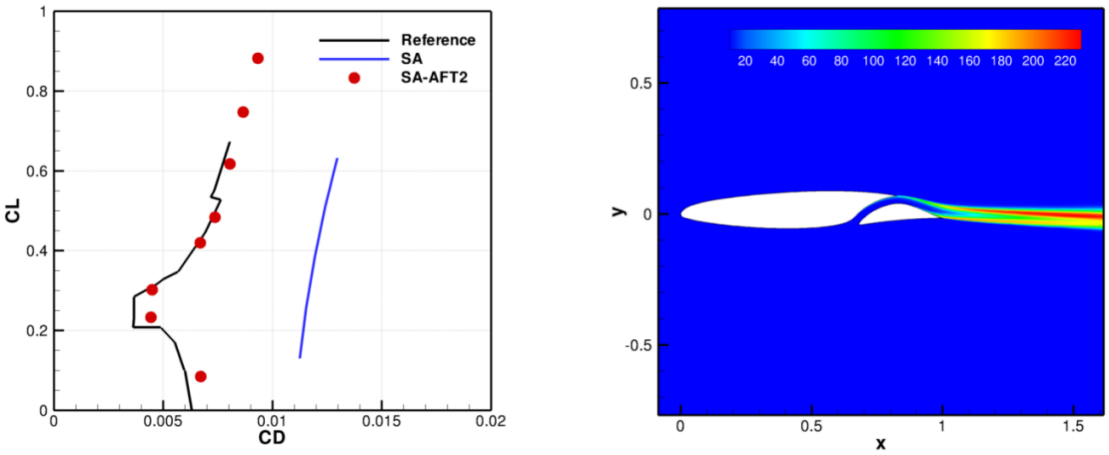

Figure 2: NSU2D-AFT2 polar comparison to reference[20] for $Mach = 0.7$, $Re = 12e6$, $Tu_\infty = 0.07\%$ **(left)**, and solution eddy viscosity contour **(right)** for the S204 SNLF Airfoil

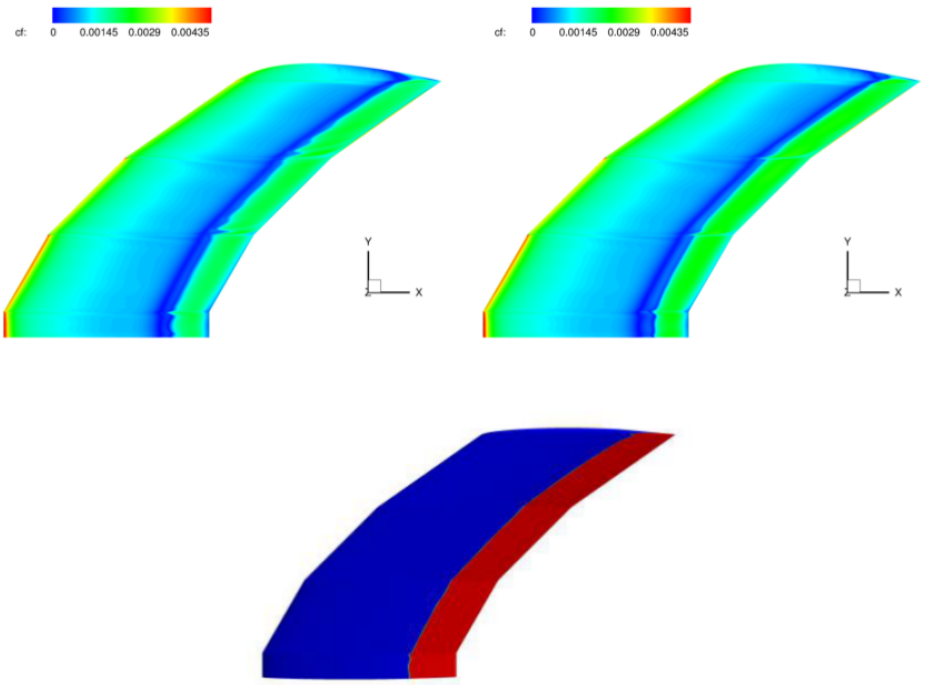

Figure 3: Upper surface transition location illustrated with skin friction distribution computed by the Menter model **(upper right)** and AFT2 model **(upper left)** compared to contour presented in reference[23] for *Mach = 0.156*, *Re = 2.7e6*, *Alpha = -2.6*

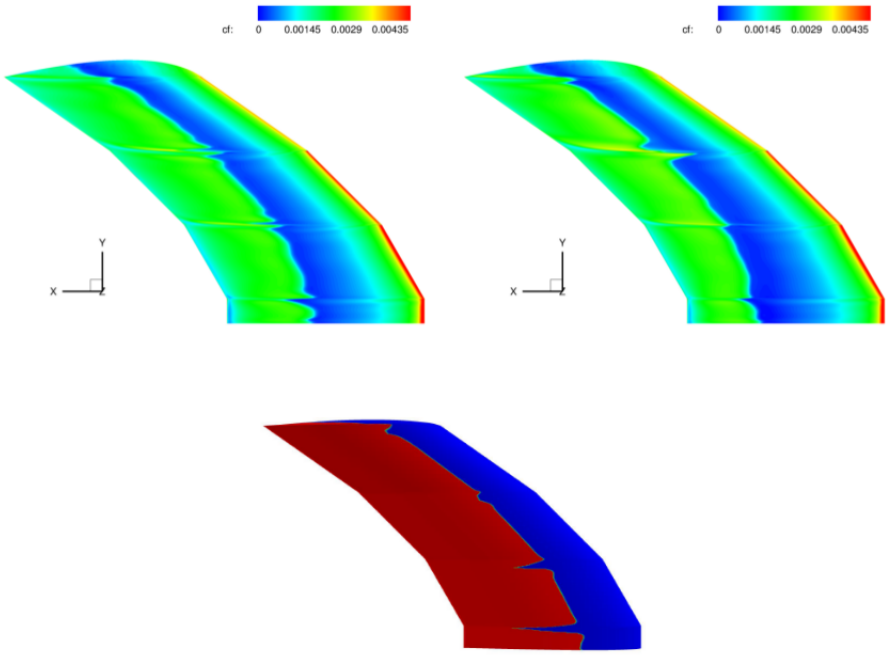

Figure 4: Lower surface transition location illustrated with skin friction distribution computed by the Menter model **(upper right)** and AFT2 model **(upper left)** compared to contour presented in reference[23] for *Mach = 0.156*, *Re = 2.7e6*, *Alpha = -2.6*

IV Two-Dimensional Analysis of the S207 Airfoil

Two-dimensional runs were performed in order to establish the correspondance between our RANS CFD predictions with the design performance of the S207 SNLF airfoil at nominal conditions. Additionally, a set of runs were performed to study the sensitivity of the airfoil performance to small variations in the slot geometry.

A. Free Transition at Nominal Conditions

An unstructured mesh was generated for the S207 airfoil using the UMESH2D mesh generator associated with the NSU2D software package,[25] and is shown as Figure 5. In total the grid has 689326 cells, and far field boundaries are located at a distance of 1000 chord lengths. Both elements have approximately 2000 surface points, and the streamwise spacing at the leading and trailing edges of each element was set to 0.02% the chord length to ensure sufficient resolution. The normal wall spacing for both elements was set as 10^{-6} chord lengths, and the growth rate of the cells in the boundary layer region was set to 1.1 in order to capture the expected thin laminar boundary layer.

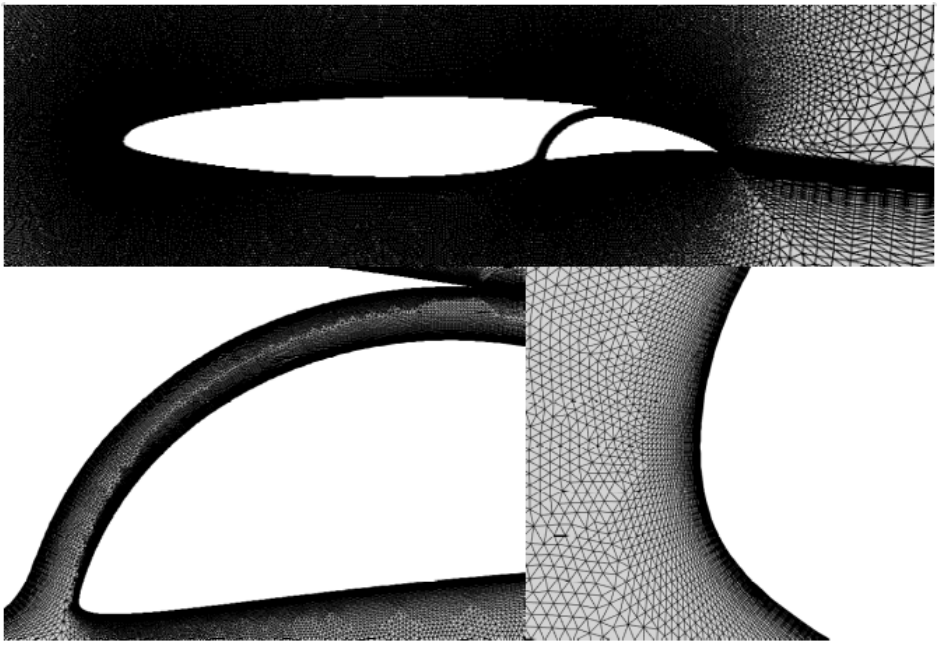

Figure 5: 2D mesh for the S207 SNLF airfoil: full configuration **(top)**, slot **(bottom left)**, and fore element leading edge **(bottom right)**

Similar to the S204, the S207 was theoretically designed and analyzed initially using Eppler and MSES.[2] Nominal angles of attack at cruise conditions are predominantly negative, with lift coefficient values falling within the range of the low-drag bucket (i.e. $0.37 < C_L < 0.74$).[2] Using the AFT2 model with a freestream turbulence value of *0.001%*, a two-dimensional simulation was run for freestream flow values of *Mach = 0.7*, *Re = 13.2e6* and *Alpha = -1.3*. The convergence history of the lift coefficient and the density residual for this case are shown in Figure 6. The residual values converged approximately seven orders of magnitude. However this was enabled by freezing the transition equation updates after 3250 cycles in order to prevent the residuals from stagnating. Comparison of the transition locations with and without freezing showed negligible differences, which justified this approach. However, the overall number of iterations to achieve deep residual convergence remains significantly higher than what is required for equivalent fully turbulent runs using the SA model alone. The drag coefficient values in the vicinity of the low-drag bucket at these flow conditions were predicted by MSES to be in the range of 27 to 29 counts of drag.[2] NSU2D computed 31.8 counts of drag at a lift coefficient of 0.658, which falls slightly lower than the upper *CL* limit of the drag bucket. The fully turbulent flow simulation of the S207 airfoil at these same flow conditions is also shown in the drag polar of Figure 6. A

few notes should be made upon examination of the differences between the fully turbulent and free transition results. The first being that the magnitude of said discrepancy is large, with the fully turbulent drag being much higher and associated lift significantly lower. Additionally, the free transition simulation much more closely aligns with design data. It is clear that the performance of the S207 is not accurately predicted without free transition modeling.

Transition and turbulence should only be present on the upper surface of the aft element.[2] Figure 7 illustrates the solution flow field quantified with eddy viscosity, and a separate Mach contour plot of the flow through the slot. It is evident from these images that laminar flow is achieved on the fore element and smooth flow through the slot is observed. Figure 8 plots the computed skin friction coefficient values for the free transition case, showing transition to occur at approximately 87% of the chord length on the upper surface of the flap.

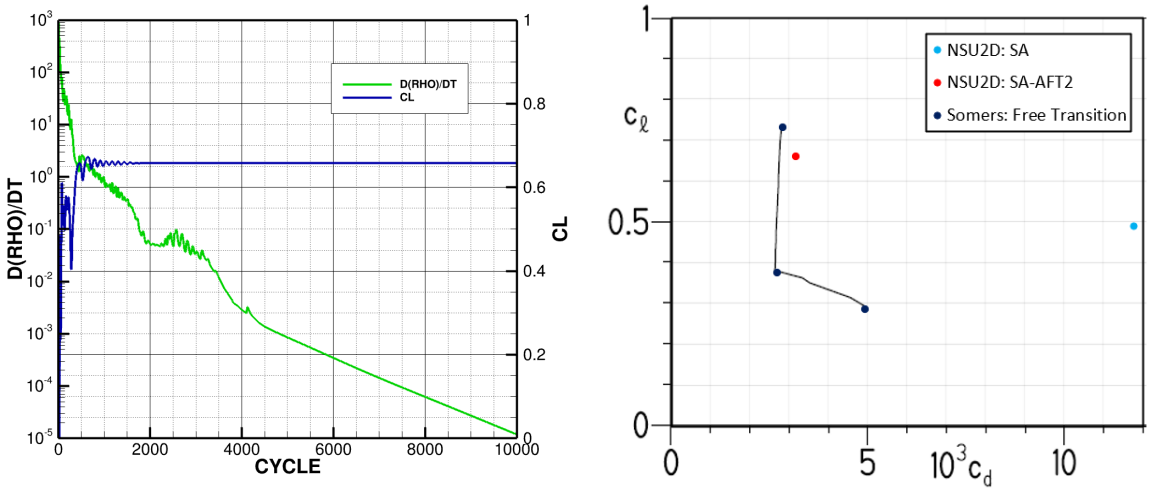

Figure 6: NSU2D results for *Mach = 0.7*, *Alpha = -1.3*, and *Re = 13.2e6*: convergence history with the AFT2 model **(left)**, and AFT2 results compared with NSU2D-SA data and reference[2] **(right)**

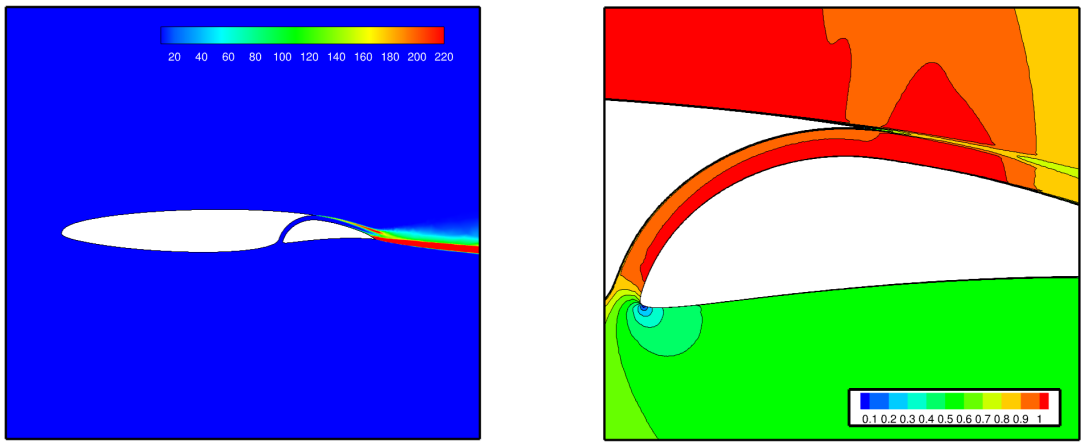

Figure 7: NSU2D-AFT flow visuals for *Mach = 0.7*, *Re = 13.2e6*, *Alpha = -1.3*: eddy viscosity solution field **(left)**, slot flow Mach contour **(right)**

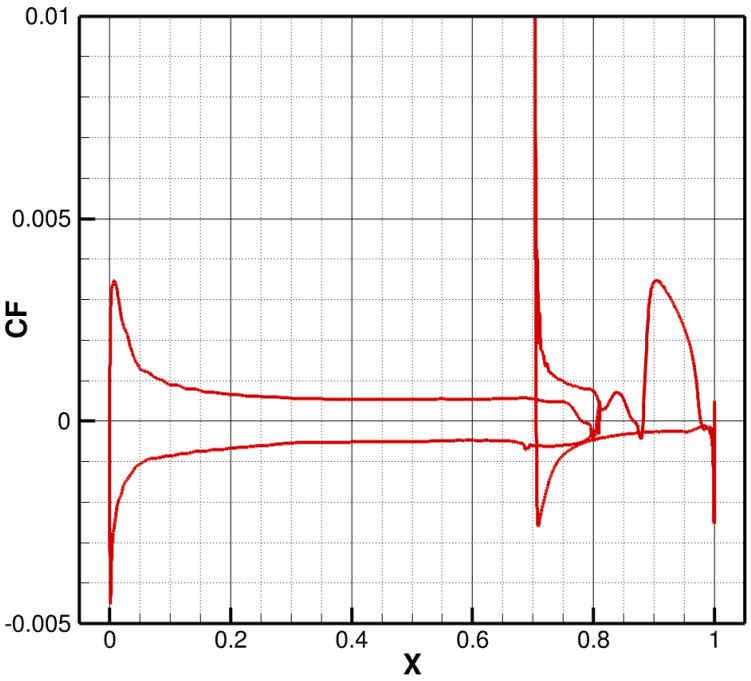

Figure 8: NSU2D-AFT2 skin friction profile for *Mach = 0.7*, *Re = 13.2e6*, *Alpha = -1.3*

B. Flap Position Sensitivity Study

The performance of SNLF airfoils is known to be particularly sensitive to geometric and associated flow changes in the slot region. Therefore, a sensitivity study of the S207 airfoil with flap position was undertaken in this work. This was motivated in part by shock wave formation in the slot region encountered in the three-dimensional configuration, as described in the subsequent section. Since these issues appeared in both transitional and fully turbulent simulations, the decision was made to perform the sensitivity study using fully turbulent simulations exclusively. Additionally, there is interest in comparing these sensitivities to expected structural displacements under load as well as manufacturing tolerances. Fully turbulent simulations offer quick insight to issues originating from small flow and geometry variations, making the capability ideal for this analysis as shock formation was of particular interest. Additionally, convergence is much easier to achieve when adverse flow characteristics are present. This was beneficial for the more extreme flap translations, as converged free transition solutions would have been difficult to obtain for these cases.

Several solutions at *Mach=0.7*, *Re=13.2e6*, and *Alpha=-1.3* were obtained. Different flap positions were used for every simulation, each with their own perturbation to the horizontal, vertical, or diagonal flap location. In all cases, a nearly identical mesh was used based on the parametric multi-element positioning capabilities built into the UMESH2D mesh generation code. A summary quantifying each solution and the associated flap translation is detailed in Table 1.

Mach contour plots comparing the baseline configuration flow characteristics to solutions acquired with aft-element translation are shown in Figure 9. Narrowing the slot with horizontal flap displacement results in shock formation near the slot exit. On the contrary, vertically translating the aft element further from the fore element predicts a shock near the entrance of the slot. With diagonal narrowing, again a shock is formed near the exit of the slot. The shock formation in these cases is accompanied by severe flow separation on the upper surface of the aft element. Vertically wide variations with no predicted shock produce flow separation on the fore element through the slot. Unsurprisingly, extreme changes in the flow field compared to that observed with the baseline configuration result in decreased values of lift and increased values of drag. Figure 10 illustrates *CL*, *CD*, and *CL/CD* values as a function of flap location. From these results, the formation of a shock and thus early flow separation appears to be highly sensitive to changes in slot geometry. To avoid compromising the SNLF performance, these results indicate that flap positioning must deviate by no more than 0.1% chord, compared to the baseline configuration. These values are well below manufacturing tolerances. Additionally, preliminary structural analysis results for the S207 wing box under gravity loads predict displacements that are well below these limits.[26] Further aerostructural analysis may be required to establish the range of expected elastic deflections for different operating conditions.

Table 1: Slot sensitivity study: flap translation summary with negative values denoting flap is closer to fore element compared to baseline

Trans. Direction	Case Number	Trans. Magnitude (% Chord)
Horizontal	1a	-0.0055
	2a	-0.0050
	3a	-0.0025
	Baseline	0.0000
	5a	0.0025
	6a	0.0050
	7a	0.0100
	8a	0.0200
Vertical	1b	-0.0055
	2b	-0.0050
	3b	-0.0025
	Baseline	0.0000
	5b	0.0025
	6b	0.0050
	7b	0.0100
	8b	0.0200
Diagonal	1c	-0.0071
	2c	-0.0035
	Baseline	0.0000
	4c	0.0035
	5c	0.0071
	6c	0.0141
	7c	0.0283

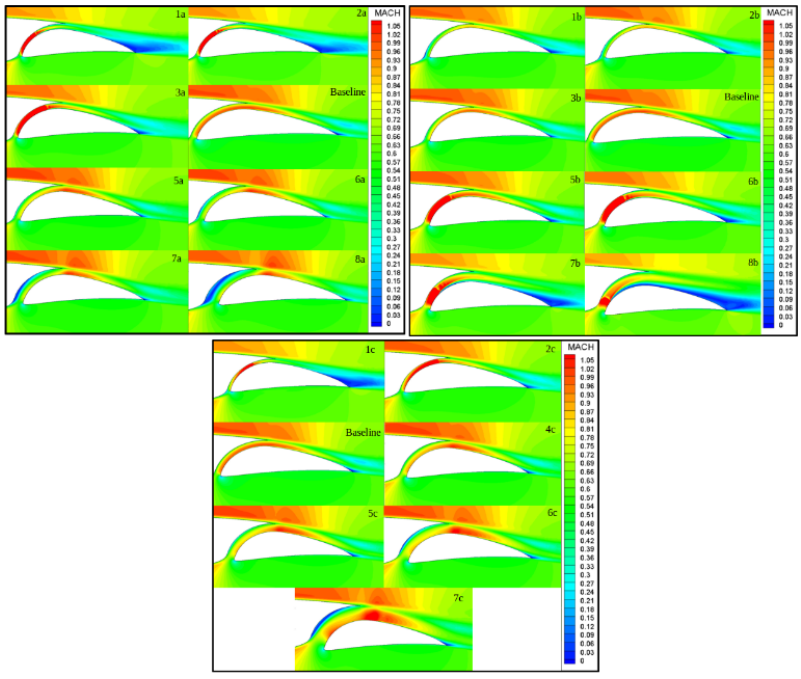

Figure 9: NSU2D-SA flow solutions for horizontal **(upper left)**, vertical **(upper right)**, and diagonal **(bottom)** variations for *Mach = 0.7*, *Re = 13.2e6*, *Alpha = -1.3*

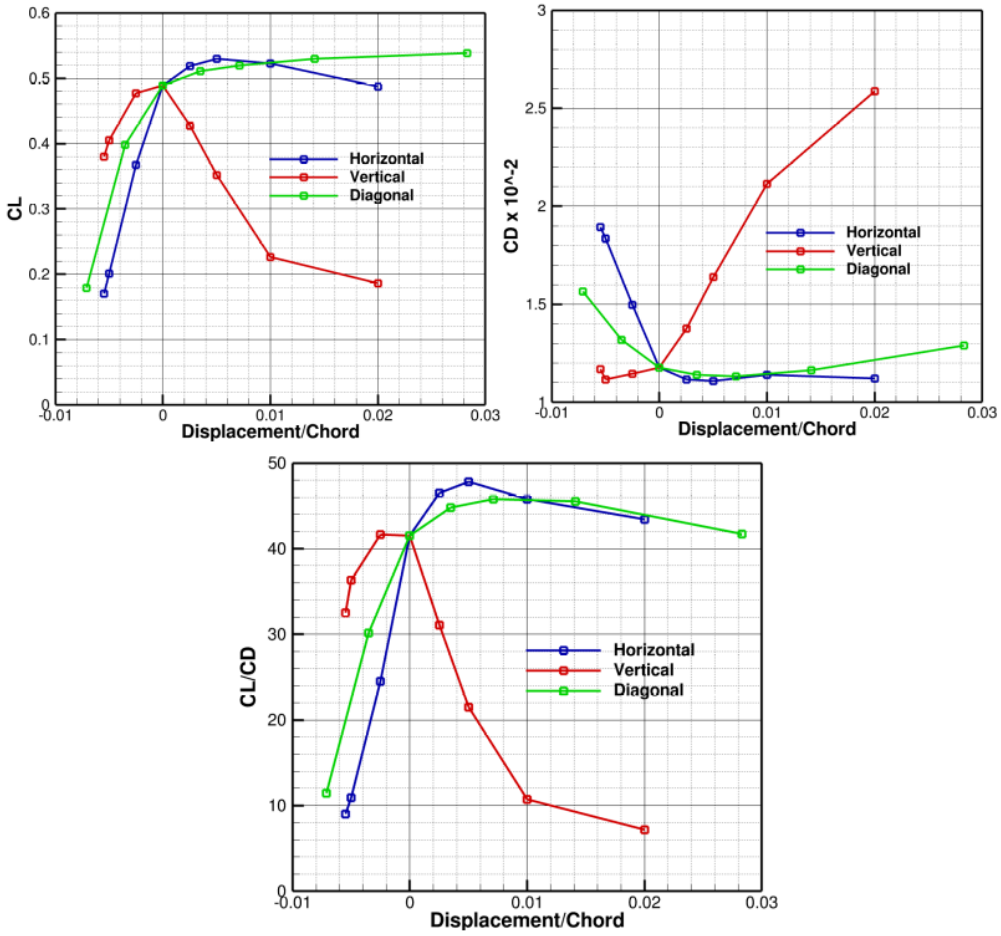

Figure 10: NSU2D-SA associated changes in *CL* **(upper left)**, *CD* **(upper right)**, and *CL/CD* **(bottom)** for variations in flap position for *Mach = 0.7*, *Re = 13.2e6*, *Alpha = -1.3*

V Results for S207 airfoil-based Aircraft

The design of the S207 aircraft was based on the 2015 version of the Boeing SUGAR aircraft, which is the ULI project's baseline comparison.[27] The fuselage and empennage were provided by Neal Harrison of the Boeing Company, and a new wing was integrated into that model. The wing was resized from $1477 ft^2$ to $1350 ft^2$ to account for the higher maximum lift coefficient of the clean SNLF airfoil,[7,28] while all other planform properties, such as aspect ratio and sweep, were maintained. The one exception is the twist, which was defined as two degrees of linear washout on the inboard panel with an additional degree in the outboard panel. The wing position was also adjusted to maintain the tail volume coefficients of the SUGAR design. A three-view of the aircraft is shown in Figure 11. Note that the strut for the truss-braced wing is not included for the current aerodynamic analysis.

A. S207 SNLF TTBW Aircraft Mesh

An unstructured mesh was generated about the S207 TTBW aircraft geometry using the Pointwise software. The mesh has approximately 72 million vertices (for a half aircraft model) and includes hybrid elements with prisms in the boundary layer and tetrahedral elements in the inviscid regions. An illustration of the mesh with details of the resolution in the slot region is shown in Figure 12.

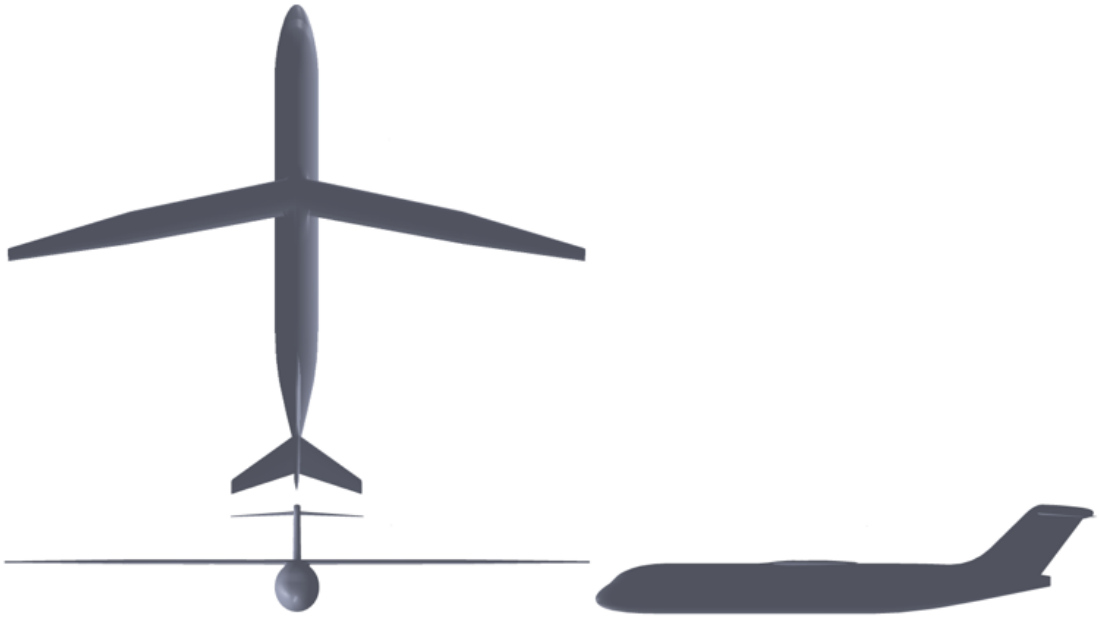

Figure 11: S207 Vehicle Geometry

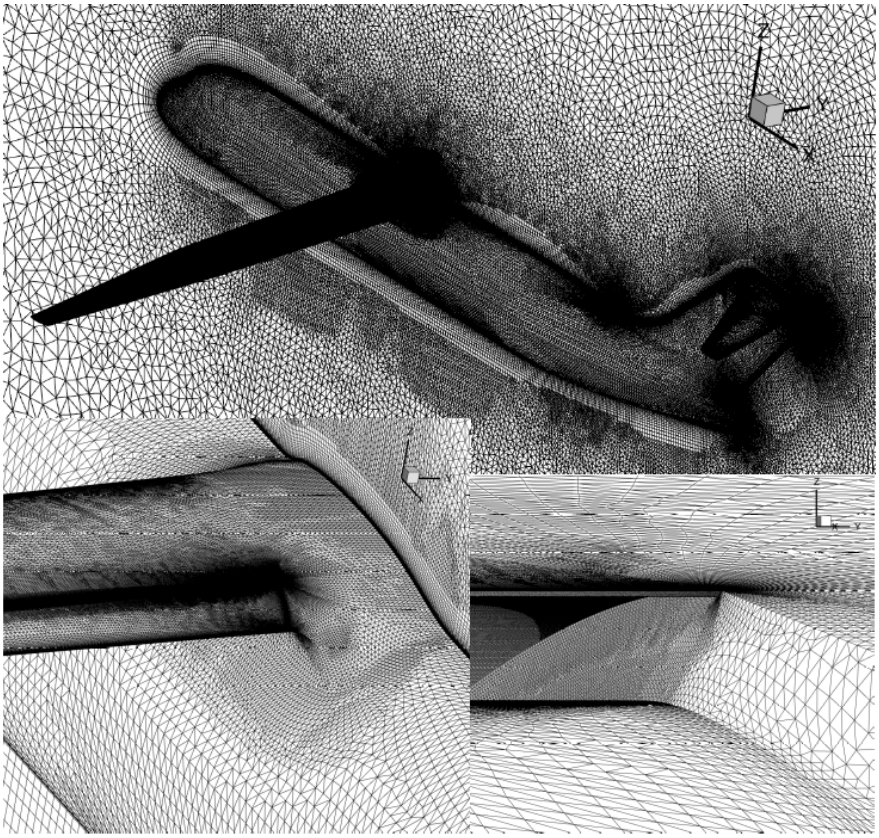

Figure 12: Full S207 vehicle mesh **(top)**, zoomed in fairing mesh **(bottom left)**, and slot refinement **(bottom right)**

B. Computational Analysis of S207 Aircraft

This mesh was used to compute a full set of polars at various Mach numbers ranging from Mach=0.2 to Mach=0.75. In all cases, fully turbulent solutions using the SA turbulence model alone, as well as free transition solutions using the coupled SA-turbulence and Menter transition models, were obtained in order to examine the effect of free transition. The Reynolds number for these cases is *1.4e6/foot*, with a wing mean aerodynamic chord (MAC) of 8.786 ft. A comparison between polars for $Mach = 0.5$ and $Mach = 0.7$ is shown in the left subfigure of Figure 13. The polars obtained for the free transition simulations display lower drag and and higher lift values than the corresponding fully turbulent simulations. This is similar to the behavior observed in two dimensions and again demonstrates the importance of free transition in the context of SNLF configurations. The spanwise lift distribution for the free-transitional runs is shown in the right subfigure of Figure 13. Here, the $Mach = 0.5$ lift distribution appears smooth, with linear to elliptic variation, whereas the higher $Mach = 0.7$ distribution shows a lift deficit outboard of the 60% span location. This unexpected behavior was traced to the presence of a shock wave in the slot at outboard span locations. Interestingly, the shock was present in both the free transition results as well as the fully turbulent results. The fully turbulent, $Alpha = 0.0$ solution for this Mach number was scrutinized at locations of *12.2%*, *61.4%*, and *73.7%* the span. Figure 14 displays Mach contours for these locations, as well as the computed surface C_p values in the slot on the surface of the fore element (flap removed for visualization). The region of low pressure indicative of supersonic flow is clearly visible over this outboard span region of the slot. From the sectional Mach contour plots, it is apparent that a shock forms in the outboard region in the slot, which in turn causes flow separation downstream on the surface of the flap due to the total pressure loss across the shock wave.

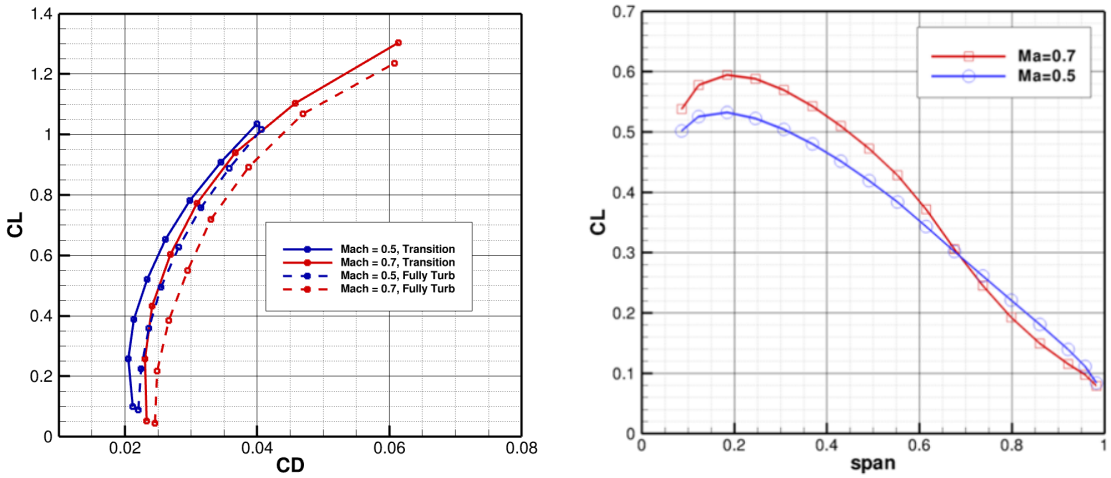

Figure 13: Configuration 1: comparisons between $Mach = 0.7$ and $Mach = 0.5$ data at $Re = 1.4e6/ft$ (MAC = 8.786 ft), $Alpha = 0.0$: polars **(left)** and spanwise *CL* computed with NSU3D-Menter **(right)**

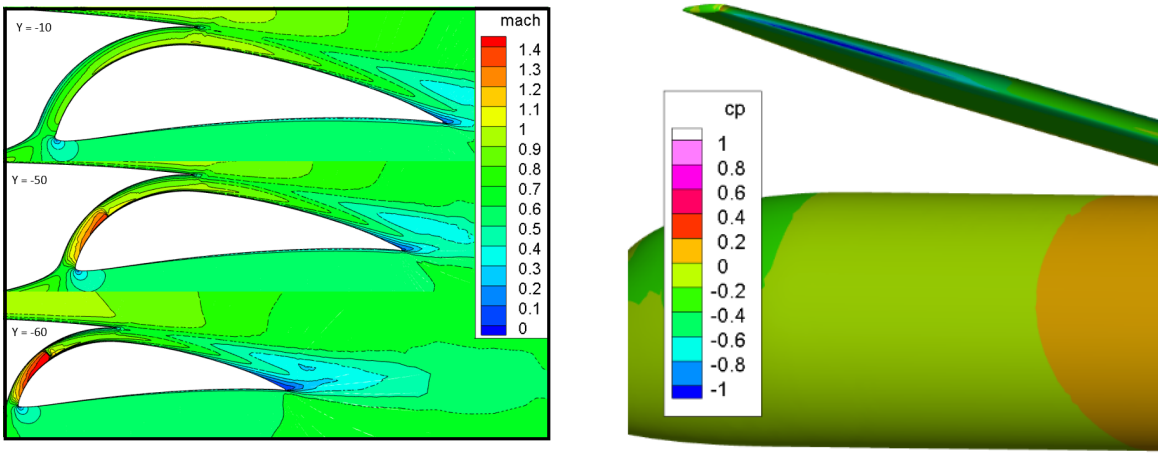

Figure 14: Configuration 1: fully turbulent flow behavior at *Mach = 0.7*, *Re = 1.4e6/ft* (MAC = 8.786 ft), and *Alpha = 0.0* for *12.2%* span **(top left)**, *61.4%* span **(middle left)**, and *73.7%* span **(bottom left)**, and computed pressure coefficients on the surface of the fore element in the slot region (flap removed for visualization) **(right)**

In the design of the three-dimensional wing, a sweep transformation was used on the S207 to define airfoil profiles parallel to the freestream, which is convenient for lofting purposes. The streamwise airfoil sections were generated by transforming the standard S207 for the local sweep of inboard and outboard panels using conical sweep transformation relations.[29,30] A miscalculation in the transformation led to an incorrect geometry for the aft element of the SNLF wing. A redesign was undertaken using the corrected transformation, and a comparison of the miscalculated and corrected coordinates is shown in Figure 15. The difference in coordinates near the entrance to the slot was 0.13 inches in the horizontal direction and 0.16 inches in the vertical direction, which is in the range of 0.1% chord. Note that this is in the range of variations that was found to have an adverse effect on airfoil performance in the 2D studies, while also being larger than manufacturing tolerances.

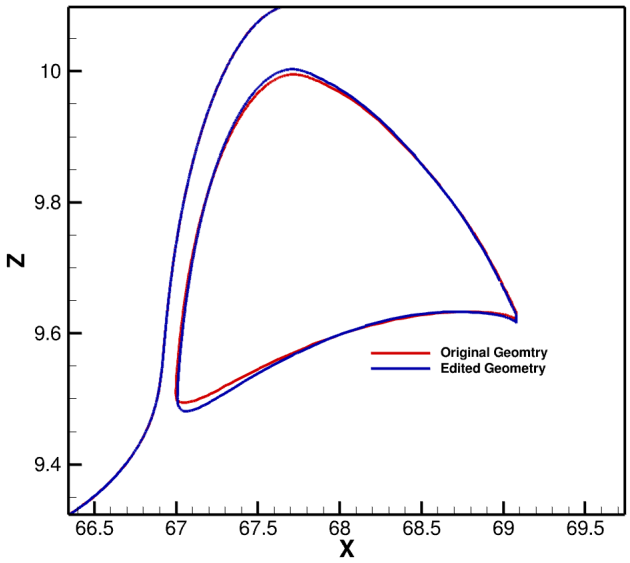

Figure 15: Flap geometry comparison between S207 SNLF TTBW vehicle configuration 1 and configuration 2 at *73.7%* span

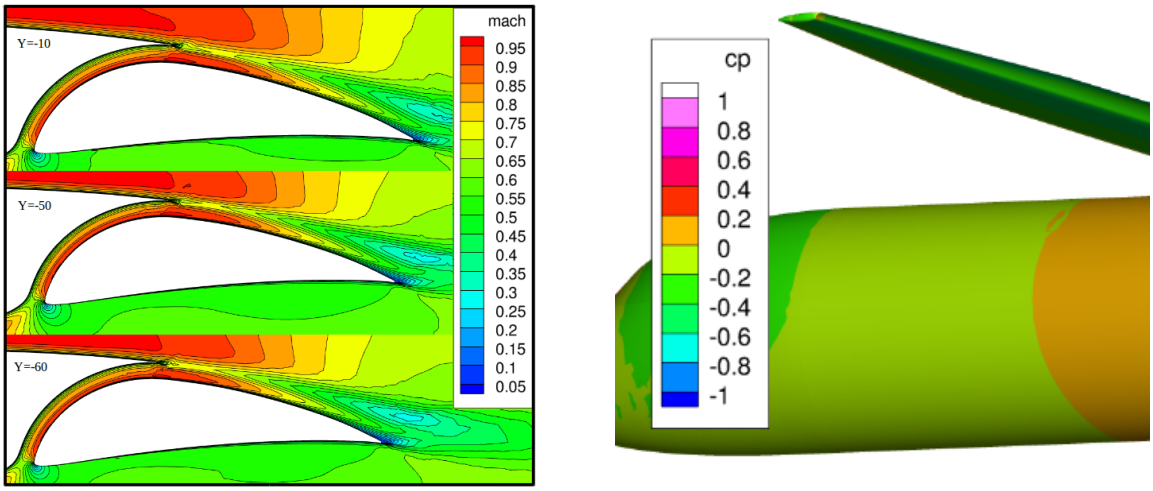

Figure 16: Configuration 2: fully turbulent flow behavior at *Mach = 0.7*, *Re = 1.4e6/ft* (MAC = 8.786 ft), and *Alpha = 0.0* for *12.2%* span **(top left)**, *61.4%* span **(middle left)**, and *73.7%* span **(bottom left)**, and computed surface pressure coefficient on surface of fore element (flap removed for visualization) **(right)**

A new mesh was generated on the redesigned geometry, using the same resolution parameters and resulting in an equivalent number of grid points of approximately 72 million. Close examination of the flow details revealed the absence of any shock formation in the slot region for both free transition and fully turbulent cases at *Mach=0.7* and 0^o angle of attack. Drag polars were again obtained using fully turbulent and free transition CFD runs for the second configuration with the Reynolds number held at *1.4e6/ft* (MAC = 8.786 ft). These drag polars are shown for all cases in Figure 17. The effect of free transition is quantified through comparison of lift curves and drag polars for *Mach = 0.5* and *Mach = 0.7* in Figure 18, showing the previously observed trends of lower drag and higher lift for the free transition solutions. Figure 19 compares the computed friction drag for the free transition runs with the fully turbulent runs in order to highlight the differences due to free transition. Here, the fully turbulent results are seen to have relatively flat friction drag profiles as a function of angle of attack, as opposed to the transitional runs, which form a low-drag bucket in the region roughly between 0^o and 3^o. The transition location predicted by the free transition model can be illustrated with the use of skin friction contours, as shown for *Mach = 0.7* and *Alpha = 0.0* in Figure 20.

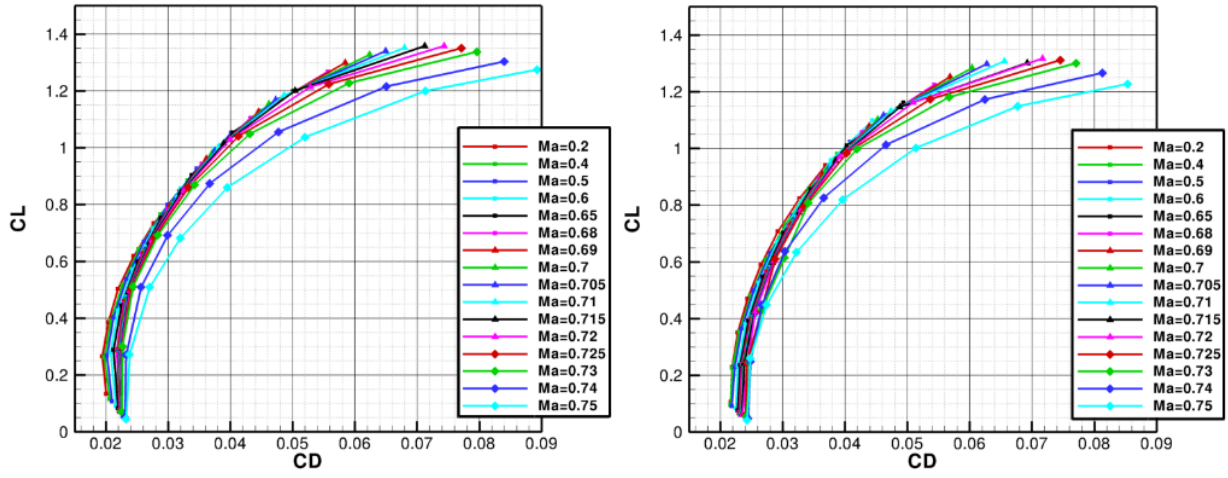

Figure 17: Configuration 2: computed drag polars for free transition (NSU3D-SA-Menter) **(left)** and fully turbulent (NSU3D-SA) runs **(right)**, *Re=1.4e6/ft*

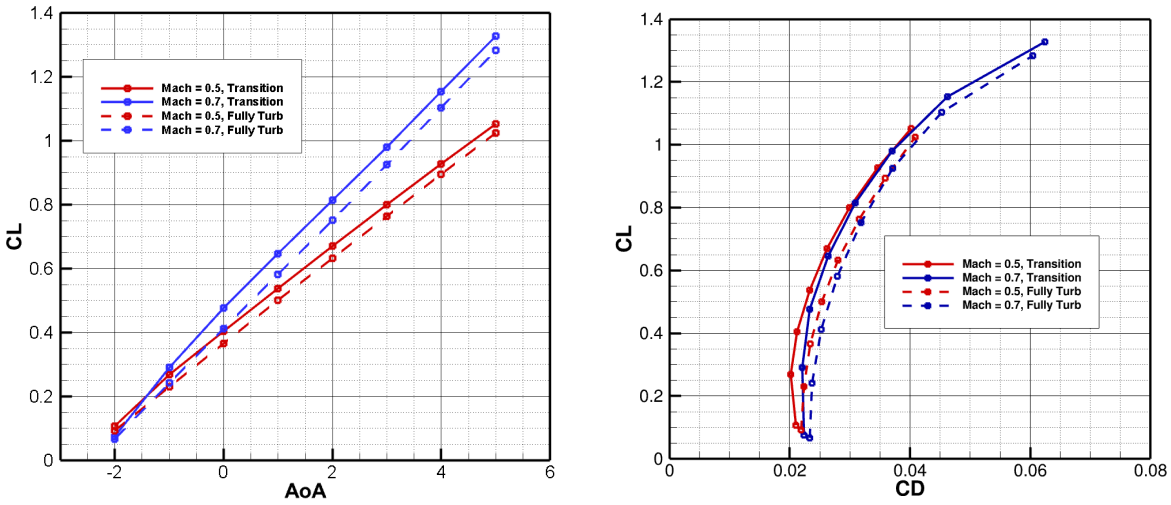

Figure 18: Configuration 2: *CL* curves **(left)** and drag polars **(right)** acquired with NSU3D-SA-Menter and NSU3D-SA for *Mach = 0.5* and *Mach = 0.7*, *Re = 1.4e6/ft*

Though success was found in eliminating the presence of any shock waves at these conditions, Figure 20 suggests that transition occurs significantly further upstream on both the upper and lower surfaces of the fore element compared to the design behavior of the S207 airfoil in two-dimensions, as discussed and shown previously in Figures 6 through 8. Further examination of the free transition simulation at *Mach = 0.7* and *Alpha = 0.0* reveals that, over the entire span, the sectional lift coefficient based on the local chord falls within the upper and lower limits of the low-drag bucket for the two-dimensional S207 airfoil, as shown in Figure 21. Additionally, the figure shows how the redesigned wing configuration achieves a smooth nearly elliptic sectional lift distribution (based on MAC), which is indicative of the absence of any shock waves in the slot region.

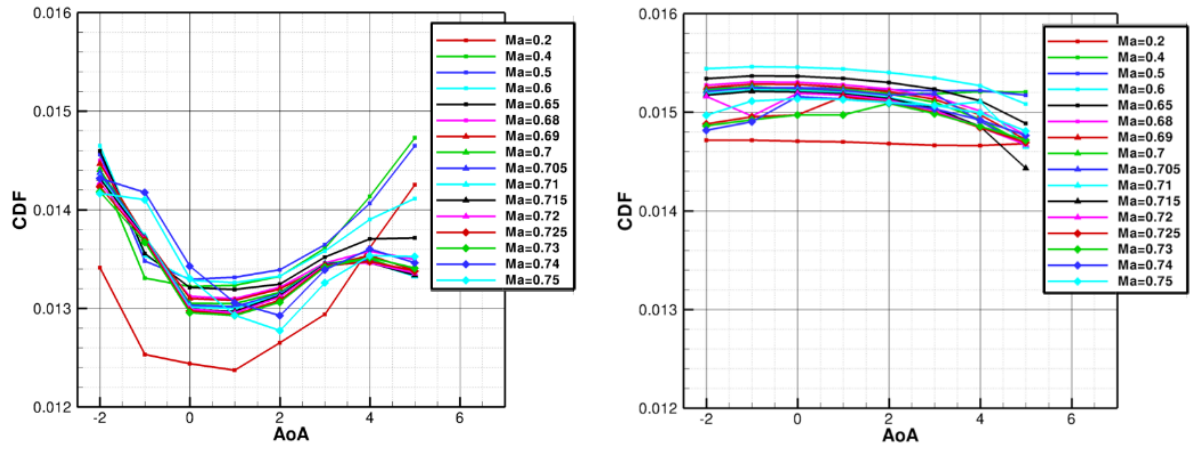

Figure 19: Configuration 2: Friction drag for various Mach numbers as a function of *Alpha* for free transition (NSU3D-SA-Menter) **(left)** and fully turbulent (NSU3D-SA) runs **(right)**, *Re=1.4e6/ft* (MAC = 8.786 ft)

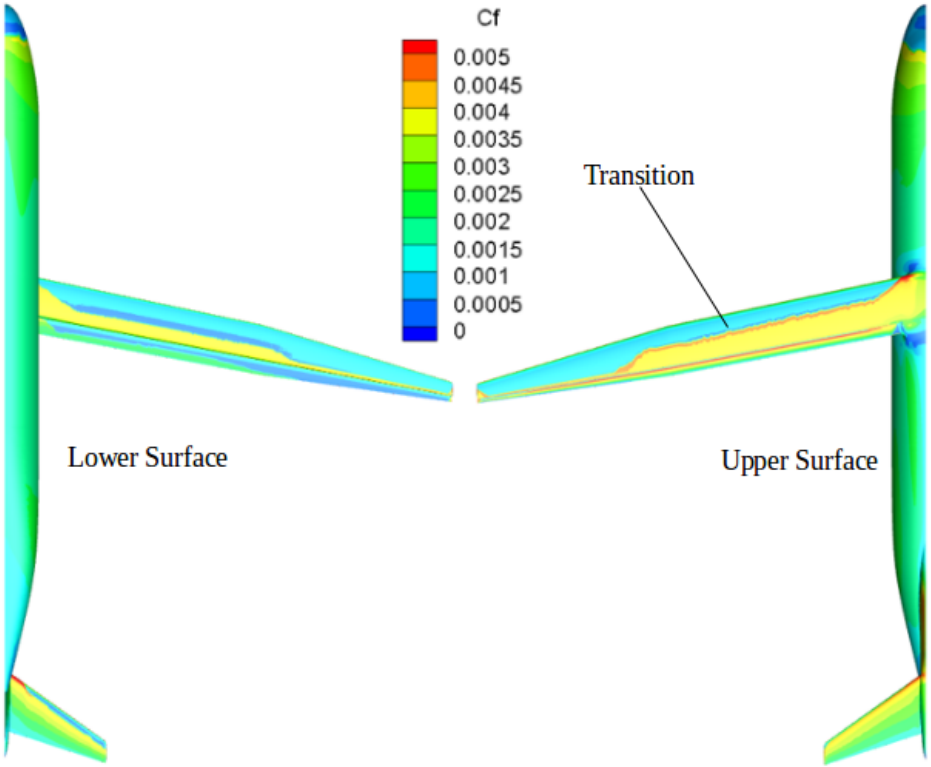

Figure 20: Configuration 2: NSU3D-SA-Menter computed skin friction profile for upper and lower surfaces at *Mach = 0.7*, *Alpha = 0.0*, and *Re = 1.4e6/ft* (MAC = 8.786 ft)

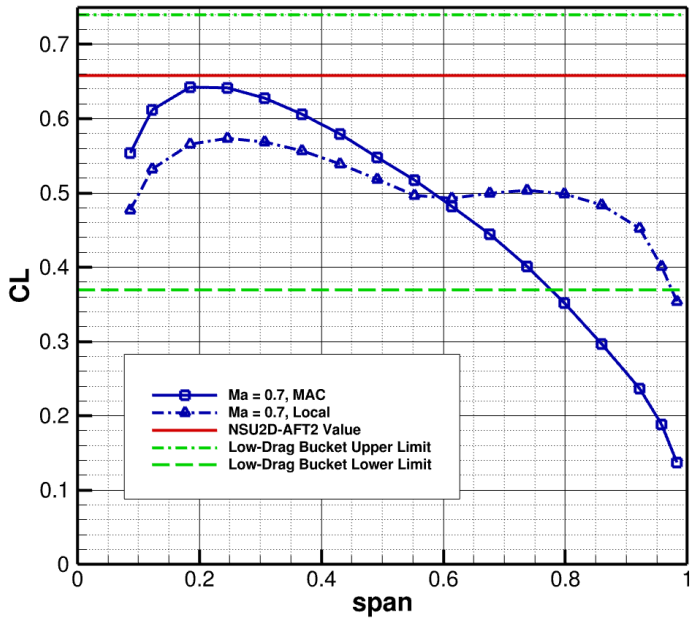

Figure 21: Configuration 2: Free transition NSU3D-SA-Menter spanwise lift at *Mach = 0.7*, *Alpha = 0.0*, and *Re = 1.4e6/ft* (MAC = 8.786 ft) compared to NSU2D-AFT2 lift computed for *Mach = 0.7*, *Alpha = -1.3*, and *Re = 13.2e6* and 2D low-drag bucket C_L limits

In order to further investigate the possible causes of early transition on this configuration, computed pressure coefficient distributions at selected spanwise stations are compared to two-dimensional results obtained on the S207 airfoil at the same conditions. In these comparisons, all simulations are performed assuming fully turbulent flow. This approach provides a means for isolating flow field differences due to geometry and/or flow conditions from differences due to possibly inconsistent transition prediction. Figure 22 illustrates the NSU3D-SA (fully turbulent) computed surface pressure for both the fore and aft elements at *Mach = 0.7* and *Alpha = 0.0*. Profiles at *8.6%*, *18.4%*, and *36.9%* span are plotted against NSU2D-SA solutions (fully turbulent) for *Mach = 0.7*, *Re = 13.2e6* and *Alpha = -1.0, -1.3*, in an effort to match the sectional lift coefficient of the 3D profile. At the *8.6%* span location, the agreement between 3D and 2D results is poor, particularly toward the trailing edge of the fore element and through the slot. Locations further spanwise at *18.4%* and *38.9%* are more consistent with 2D results with the exception of the slot region. The higher slot pressure is also seen on the upper surface of the flap. Additionally, the favorable pressure gradient along the upper surface of the fore element, which is responsible for maintaining laminar flow, is less pronounced in the 3D profiles, particularly for the most inboard sections. Note that these comparisons do not include any sweep corrections, which would be of the order of 5% given the wing sweep angle of 12.5^o. These results suggest that either the inboard airfoil sections must be modified to more closely match the 2D design properties of the S207 airfoil, or that the flow experiences three dimensional effects in these regions. At these flow conditions, CFD computations predict flow separation on the upper surface of the fuselage in the region of the wing-fuselage fairing (see Figure 20). One possibility is that this flow separation may contaminate the expected laminar flow on the wing. However, further investigation is required to clarify the origin of the observed early transition in the current simulations.

VI Conclusions

Reynolds averaged Navier-Stokes analysis of the S207 slotted, natural-laminar-flow airfoil at cruise conditions has been performed in two dimensions utilizing a transition model. The results are in good agreement with previously published MSES results used to design the airfoil.[2] The results predict entirely laminar flow over the fore element with transition occurring on the upper surface of the aft element at approximately 87% of the chord length. A total of 31.8 counts of drag is predicted for an angle of attack in the low drag region. A sensitivity study of the S207 flap position has shown that flap displacements of the order of 0.1% chord can have a detrimental impact on airfoil performance. Application of RANS CFD to the three-dimensional S207 aircraft geometry has shown the potential for discovering design inconsistencies that can adversely impact performance. Notably, in many cases the use of fully turbulent flow simulations can be used to quickly identify unexpected flow physics for SNLF configurations, and can also be used to isolate effects due to geometric changes from differences due to free transition prediction. This work constitutes one step in the effort to design and analyze an efficient SNLF-based TTBW aircraft configuration. Although the most recent configuration analyzed in this work displayed superior performance compared to the initial configuration, the predicted extent of laminar flow falls short of the design objectives for this SNLF wing, and work is currently underway to better understand the root causes of these discrepancies. Future work will also include coupled aero-structural simulations in an effort to understand if structural deflections under flight loads have the potential to adversely impact aerodynamic performance for these configurations.

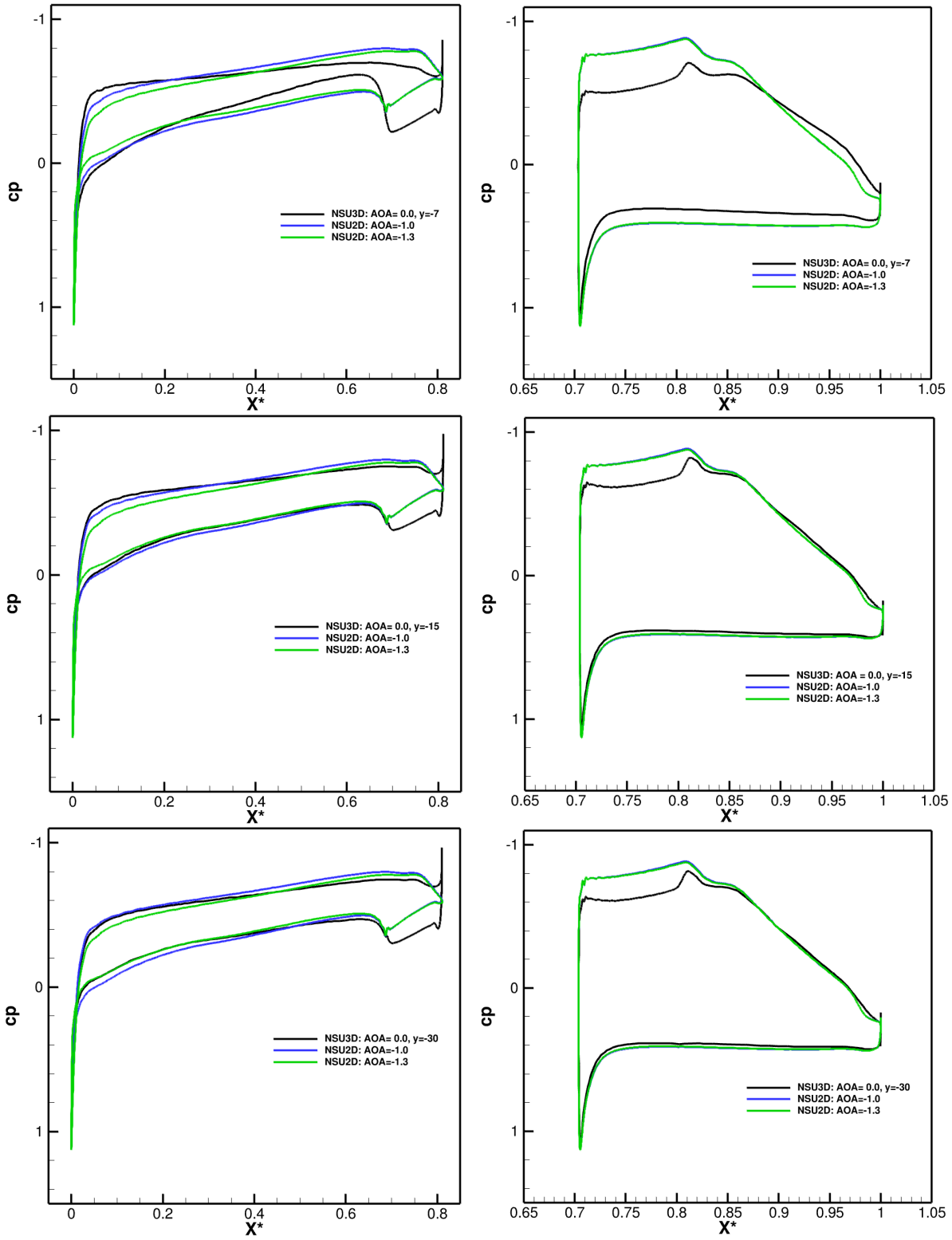

Figure 22: Configuration 2: NSU3D-SA fore **(left)** and aft **(right)** pressure coefficient profiles for *Mach = 0.7*, *Re = 1.4e6/ft* (MAC = 8.786 ft), and *Alpha = 0.0* compared to NSU2D-SA solutions at *Mach = 0.7*, *Re = 13.2e6*, and both *Alpha = -1.0, -1.3*. Analysis is made at *8.6%* span **(top)**, *18.4%* span **(middle)**, and 36.9% span **(bottom)**

Acknowledgments

This work is supported by the National Aeronautics and Space Administration (NASA) University Leadership Initiative (ULI) "Advanced Aerodynamics Design Center for Ultra-Efficient Commercial Vehicles" (Award NNX17AJ95A) led by the University of Tennessee at Knoxville. Thanks are extended to the NASA ULI Vision-Vehicle Integration Subgroup. This work would not have been possible without their consistent collaboration efforts. Additional thanks is given to both the University of Wyoming ARCC and the NCAR Wyoming Supercomputer Alliance for computer time.

References

[1] NASA Aeronautics, "Strategic Implementation Plan: 2019 Update," 2019.

[2] D. Somers, "Design of a Slotted, Natural-Laminar-Flow Airfoil for Transport Aircraft," NASA/CR-2019-220403, June, 2019.

[3] M. Maughmer, J. Coder and D. Somers, "Exploration of a slotted, natural-laminar-flow airfoil concept," AIAA Paper 2018-3815, 2018 Applied Aerodynamics Conference, July 25-29, Atlanta, GA.

[4] J. Coder, M. Maughmer and D. Somers, "Theoretical and experimental results for the S414, slotted, natural-laminar-flow airfoil," *Journal of Aircraft*, Vol. 51, No. 6, Nov. 2014, pp. 1883–1890.

[5] J. Coder and D. Somers, "Design of a slotted, natural-laminar-flow airfoil for commercial aircraft applications," *Aerospace Science and Technology*, Vol. 106, Nov. 2020.

[6] M. Bradley and C. Droney, "Subsonic Ultra Green Aircraft Research Phase II: N+4 Advanced Concept Development," NASA/CR-20120217556, May, 2012.

[7] P. Camacho, K. Pham, L. Chou, N Harrison and A. Khodadoust, "Progress on aerodynamic performance analysis of SNLF transonic truss-braced wing," AIAA Paper 2020-1025, 2020 AIAA SciTech Forum, Jan. 6-10, Orlando, FL.

[8] J. Coder, "Advanced Aerodynamic Design Center for ultra-Efficient Commercial Vehicles: ARMD Strategic Thrust: Ultra-Efficient Commercial Vehicles (Thrust 3A)," Presented at the University Leadership Initiative Annula Review, Sep., 2021.

[9] W. Valarezo and D. Mavriplis, "Navier-Stokes applications to high-lift airfoil analysis," *Journal of aircraft*, Vol. 32, No. 3, 1995, pp. 618–624.

[10] K. Mani and D. Mavriplis, "Unstructured mesh solution techniques using the NSU3D solver," 2014, AIAA Paper 2014-0081, 52nd Aerospace Sciences Meeting, January 2014.

[11] P. Spalart and S. Allmaras, "A one-equation turbulence model for aerodyanamic flow," *Recherche Aerospatiale*, 1994, pp. 5–21.

[12] M. Park, K. Laflin, M. Chaffin, N. Powell and D. Levy, "CFL3D, FUN3D, and NSU3D Contributions to the Fifth Drag Prediction Workshop," *Journal of Aircraft*, Vol. 51, No. 4, July 2014, pp. 1268–1283.

[13] D. Mavriplis, Z. Yang and M. Long, "Results Using NSU3D for the First Aeroelastic Prediction Workshop," AIAA Paper 2013-0786, 51st AIAA Aerospace Sciences Meeting, Jan. 7-10, 2013, Dallas/FT. Worth, TX.

[14] D. Mavriplis, M. Long, T. Lake and M. Langlois, "NSU3D Results for the Second AIAA High lift Prediction Workshop," *Journal of Aircraft*, Vol. 52, No. 4, Aug. 2015, pp. 1063–1081.

[15] J. Coder, "Enhancement of the Amplification Factor Transport Transition Modeling Framework," AIAA Paper 2017-1709, 2017 AIAA SciTech Forum, Jan. 9-13, Grapevine, TX.

[16] J. Coder, T. Pulliam and J. Jensen, "Contributions to HiLiftPW-3 Using Structured, Overset Grid Methods," AIAA Paper 2018-1039, 2018 AIAA SciTech Forum, Jan. 8-12, Kissimmee, FL.

[17] Z. Yang and D. Mavriplis, "Implmentation of transition modeling for analysis and optimization of two-dimensional airfoil problems," AIAA Paper 2019-0293, 2019 AIAA SciTech Forum, Jan. 7-11, San Diego, CA.

[18] F. Menter, P. Smirnov, T. Liu and R. Avancha, "A One-Equation Local Correlation-Based Transition Model," *Flow, Turbulence and Combustion*, Vol. 95, No. 4, 2015, pp. 583–619.

[19] R. Nichols, "Addition of a Local Correlation-Based Boundary Layer Transition model to the CREATETM-AV Kestrel Unstructured Flow Solver," 2019, AIAA Paper 2019-1343, 2019 AIAA SciTech Forum, Jan. 7-11, San Diego, CA.

[20] D. Somers, "Design of a Slotted, Natural-Laminar-Flow Airfoil for Business Jet Applications," NASA/CR-20120217559, July, 2012.

[21] R. Petzold and R. Radespiel, "Transition on a wing with spanwise varying crossflow and linear stability analysis," *AIAA Journal*, Vol. 53, No. 2, Feb. 2015, pp. 321–255.

[22] D. Mavriplis, Z. Yang and E. Anderson, "Development of an analysis and optimization tool for slotted wing natural-laminar-flow aircraft," AIAA Paper 2020-1292, 2020 AIAA SciTech Forum, Jan 6-10, Orlando, FL.

[23] J. Coder, "Further Development of the Amplification Factor Transport Transition Model for Aerodynamic Flows," AIAA Paper 2019-0039, 2019 AIAA SciTech Forum, Jan. 7-11, San Diego, CA.

[24] Z. Yang and D. Mavriplis, "Improved Fluid-Structure Interface for Aeroelastic Computations with Non-Matching Outer Mold Lines," AIAA Paper 2021-0844, 2021 AIAA SciTech Forum, Virtual Event, Jan 2021.

[25] D. Mavriplis, "An advancing front Delaunay triangulation algorithm designed for robustness," *Journal of Computational Physics*, Vol. 117, No. 1, 1995, pp. 90–101.

[26] A. Bottai, R. Campbell and M. Jonson, "Vibrations of a high-aspect ratio, two element wing," 2022, AIAA Paper 2022-XXXX, To be presented at AIAA SciTech Forum, San Diego, CA., Jan 3-7, 2022.

[27] M. Bradley and C. Droney, "Subsonic Ultra Green Aircraft Research: Phase 2. Volume 2; Hybrid Electric Design Exploration," NASA/CR-2015-218704/Volume II, NASA Langley Research Center, Hampton, VA, April 2015.

[28] L. Metkowski and M. Maughmer, "Winglet and Strut Configuration Study for a Slotted, Natural-Laminar-Flow Strut-Braced Transport Aircraft," AIAA Paper 2021-0843, AIAA Scitech Forum 2021, Virtual event, January 2021.

[29] K. Risse, F. Schueltke and E. Stumpf, "Progress on aerodynamic performance analysis of SNLF transonic truss-braced wing," AIAA Paper 2014-0023, AIAA SciTech 2014 Forum, Jan. 1014.

[30] R. Cummings, W. Mason, S. Morton and D. McDaniel, "Applied Computational Aerodynamics: A Modern Engineering Approach,," 2015, Cambride Aerospace Series, New York NY.